arXiv:1411.2092v2 [cond-mat.soft] 11 Jan 2015

Differential capacitance of the electric double layer: The interplay between ion finite size and dielectric decrement

Yasuya Nakayama[1, a)] and David Andelman[2, b)]
[1)] *Department of Chemical Engineering, Kyushu University, Nishi-ku, Fukuoka 819-0395, Japan*
[2)] *Raymond and Beverly Sackler School of Physics and Astronomy, Tel Aviv University, Ramat Aviv 69978, Tel Aviv, Israel*

(Dated: 13 January 2015)

We study the electric double layer by combining the effects of ion finite size and dielectric decrement. At high surface potential, both mechanisms can cause saturation of the counter-ion concentration near a charged surface. The modified Grahame equation and differential capacitance are derived analytically for a general expression of a permittivity $\varepsilon(n)$ that depends on the local ion concentration, n, and under the assumption that the co-ions are fully depleted from the surface. The concentration at counter-ion saturation is found for any $\varepsilon(n)$, and a criterion predicting which of the two mechanisms (steric vs. dielectric decrement) is the dominant one is obtained. At low salinity, the differential capacitance as function of surface potential has two peaks (so-called camel-shape). Each of these two peaks is connected to a saturation of counter-ion concentration caused either by dielectric decrement or by their finite size. Because these effects depend mainly on the counter-ion concentration at the surface proximity, for opposite surface-potential polarity either the cations or anions play the role of counter-ions, resulting in an asymmetric camel-shape. At high salinity, we obtain and analyze the crossover in the differential capacitance from a double-peak shape to a uni-modal one. Finally, several nonlinear models of the permittivity decrement are considered, and we predict that the concentration at dielectrophoretic saturation shifts to higher concentration than those obtained by the linear decrement model.

I. INTRODUCTION

The behavior of ions in liquids, or more specifically, in aqueous solutions near charged surfaces, largely contributes to our understanding of colloidal interactions[1,2], transport in nano- and micro-pores[3,4], and electrochemical processes[5]. Traditionally, the ionic profiles have been calculated using the Poisson–Boltzmann (PB) model[1,2], which includes electrostatic interactions and entropy of mobile ions dispersed in a continuum medium of uniform permittivity, ε. The PB model captures the formation of the so-called electric double layer (EDL) close to a charged surface, where the counter-ions are loosely associated with the surface. At small surface-charge densities, the PB model is quite successful in explaining qualitatively many experimental results. However, at high surface-charge densities and for multivalent counter-ions, the PB model fails to describe the EDL even on a qualitative level[6], and other theories that take into account charge correlations and fluctuations, have been proposed[7–13].

Experiments on differential capacitance at low salt concentrations indicate that the EDL width is a decreasing function of the surface potential at low surface charge, in accord with the PB predictions. However, the PB does not predict correctly the increase in the EDL width with the surface potential at higher surface charge[14–16]. One attempt to explain this qualitative non-PB change of the EDL width was to include steric interactions between the (solvated) ions[17–24] in the PB model. In such a *sterically-modified PB* (smPB) model, the saturation of the counter-ion build-up at the surface reaches closed-packing density at high potentials. The model further predicts an increase of the EDL width with the surface charge (or equivalently with surface potential), at high surface charge conditions, in qualitative accord with experiments.

A second source of counter-ion saturation is caused by the dielectric decrement characteristic to ionic solutions, and is due to the effective polarizability of hydrated ions[17,25–30]. This effective polarizability is related to the presence of a hydration shell around ions in addition to the dielectric hole created by the ions themselves. Since ions usually have smaller dielectric constant than water, inclusion of an ion in water creates a dielectric hole that reduces the dielectric constant of the solution. However, for small and simple ions such as halides, this effect does not have a substantial contribution to the net dielectric decrement. A more significant effect is due to the hydration shell formed by water molecules in the immediate proximity to an ion. In this layer, the polar water molecules are largely oriented along the electrostatic field created by the ion, reducing the orientational polarizability and leading to a rather pronounced dielectric decrement.

The effective polarizability of hydrated ions in relation with the EDL capacitance was first analyzed by Bikerman[17], who predicted a shift in the electrocapillary maximum due to the asymmetric effective polarizabilities be-

[a)] Electronic mail: nakayama@chem-eng.kyushu-u.ac.jp
[b)] Electronic mail: andelman@post.tau.ac.il

tween the cations and anions. Depletion of a polyelectrolyte caused by dielectric decrement near the surface was pointed out by Biesheuvel[26], and the broadening of EDL by the dielectric decrement in multivalent ions and mixed electrolytes was reported in Refs. 29 and 30.

The saturation of counter-ion concentration that originates from the reduced permittivity close to the surface is called *dielectrophoretic saturation*, and was analyzed for solutions containing only counter-ions that balance the surface charges[27], as well as when salt was added to the solution[28]. First, it was shown that the dielectric decrement can cause a counter-ion saturation at the surface even without including the effect of ion finite size[27]. Later, it was pointed out that when the dielectric decrement is large, the dielectrophoretic saturation will be the dominant effect even when the ion finite size is taken into account. Furthermore, the non-monotonic variation of the differential capacitance with the surface charge can be ascribed not only to the ion finite size as predicted by the smPB model, but also to the dielectric decrement[28].

Since the counter-ion saturation at high surface charge can result from two different origins, the following two points should be elucidated. (i) Finding a general criterion to determine the dominant mechanism (steric or dielectrophoretic) for the counter-ion saturation for general nonlinear permittivity decrement; (ii) Combining the effects of dielectric decrement and ion finite size in order to analyze the differential capacitance, not only for the case of dielectrophoretic counter-ion saturation, but also for the sterically-dominant one.

Another issue that needs further attention is the high salt regime. As the salt concentration increases, the range of the surface potential where the PB model can be applied becomes smaller, and the counter-ion concentration reaches a saturation value even at rather low values of the surface potential. Using the smPB model[20], a uni-modal (or bell-shape) differential capacitance was predicted at high salt concentration above a threshold, $n_b > 1/(8a^3)$, where n_b is the salt concentration and a is the lattice size, which roughly corresponds to the solvated ion size[31]. We note that a similar bell-shape differential capacitance has been observed experimentally in ionic liquids[32], while another type of bell-shape capacitance was predicted at an electrified oil/water interface due to large organic ions[33,34]. However, the additional effect of dielectric decrement on the emergence of the bell-shaped differential capacitance has not yet been explored. For ionic solutions, the dielectric decrement at high salt concentrations can have a strong effect and, hence, change the camel-shape to bell-shape crossover of the differential capacitance.

In this paper, we study the ionic behavior of an aqueous electrolyte solution in the proximity of a surface having a constant charge density or an externally controlled surface potential. Our treatment is based on mean-field theory that includes both steric ionic effects and dielectric decrement (dielectrophoretic). The model is presented in Sec. II, while in Sec. III, a criterion for the dominant saturation of counter-ion concentration is found to be ionic specific. We also present an expression for the modified Grahame equation in Sec. III, and for the differential capacitance in Sec. IV, as applicable for general $\varepsilon(n)$ and finite ionic size. We find that the EDL width exhibits a non-monotonic variation with the surface charge, both for steric saturation and dielectrophoretic one, as is presented in Secs. IV A and IV B. In Sec. IV C, based on analytic results and numerical solutions, we explore the combined effect of dielectric decrement and ion finite size on the differential capacitance behavior, ranging from a camel-shape at low salt concentrations to bell-shape at high salt concentrations. Furthermore, corrections due to nonlinear permittivity decrement are examined in Sec. V, because they can be rather substantial at high salinity.

II. MODEL

We consider a monovalent 1:1 electrolyte solution with bulk salt concentration $n_b = n_b^+ = n_b^-$. The aqueous solution occupies the $z > 0$ region, and is in contact with a planar surface located at $z = 0$. This plane has a constant charge density (per unit area), σ, or, equivalently is held at a constant surface potential, ψ_s. The mean-field free energy is expressed in terms of the ion number densities (per unit volume), $n_\pm(z)$, and electrostatic potential $\psi(z)$, and reads[19,27]

$$\begin{aligned} F[n_\pm,\psi] = &\int_0^\infty \mathrm{d}z \left[-\frac{1}{2}\varepsilon_0\varepsilon(n_\pm)\left|\psi'\right|^2 + e(n_+ - n_-)\psi\right] \\ &+ k_BT\int_0^\infty \mathrm{d}z\, \left[n_+\ln(n_+a^3) + n_-\ln(n_-a^3)\right] \\ &+ \frac{k_BT}{a^3}\int_0^\infty \mathrm{d}z\, \phi_w \ln\phi_w, \end{aligned} \tag{1}$$

where $\psi' = \mathrm{d}\psi/\mathrm{d}z$, e is the electronic charge, ε_0 is the vacuum permittivity, $\varepsilon(n_\pm)$ is the relative permittivity that depends in our model on the local ion density $n_\pm(z)$, and, hence, implicitly on the distance z from the surface, $\phi_w(z) = 1 - a^3\sum_{\alpha=\pm} n_\alpha$ is the solute (water) volume fraction, a is the lattice spacing that is roughly equal to the solvated ion diameter, k_B is the Boltzmann constant, and T is the temperature.

The Euler–Lagrange equations determining the electrostatic potential and ion concentrations are obtained by taking the variation with respect to $n_\pm$ and ψ of the excess free energy defined from Eq. (1) to be $\Delta F = F[n_\pm,\psi] - F[n_b,0]$. These equations are written as:

$$\ln\frac{n_b}{\phi_b} = \ln\frac{n_\pm}{\phi_w} \pm \frac{e\psi}{k_BT} - \frac{\varepsilon_0}{2k_BT}\frac{\partial\varepsilon}{\partial n_\pm}\left|\psi'\right|^2, \tag{2}$$

$$\frac{\mathrm{d}}{\mathrm{d}z}\Big(\varepsilon_0\varepsilon(n_\pm(z))\psi'\Big) = -e(n_+ - n_-), \tag{3}$$

where the volume fraction of bulk water is

$$\phi_b = 1 - 2a^3n_b. \tag{4}$$

From the electro-chemical potential equality of Eq. (2), the ion concentrations can be expressed as

$$n_{\pm}(z) = \frac{\rho_{\pm}}{\phi_b + a^3(\rho_+ + \rho_-)}\,, \tag{5}$$

$$\rho_{\pm}(z) = n_b \exp\left(\mp\frac{e\psi}{k_BT} + \frac{\varepsilon_0}{2k_BT}\frac{\partial\varepsilon}{\partial n_{\pm}}\,|\psi'|^2\right)\,, \tag{6}$$

where $\rho_{\pm}(z)$ is another ionic profile defined to make the above expressions look simpler. The boundary condition at the $z = 0$ surface is obtained from the charge neutrality condition:

$$-\varepsilon_0\varepsilon_s\psi'_s = \sigma\,, \tag{7}$$

where σ is the surface charge density, $\varepsilon_s = \varepsilon(n_{\pm}(0))$ is the extrapolated value of the permittivity at the $z = 0$ surface, and $\psi'_s = \mathrm{d}\psi/\mathrm{d}z|_s$ is also evaluated at the same surface. Moreover, $\psi' = 0$ is imposed at $z \to \infty$ (no electric field at infinity).

One of the well-known attempts to go beyond the PB treatment was to consider a surface layer called the Stern layer[35] with reduced dielectric constant and also to account for specific adsorption of ions on the surface due to non-electrostatic ion-surface interactions. The Stern proximity layer was introduced to explain some experimental observations which cannot be explained by the conventional PB model, that are magnitude of the capacitance [36,37] and its non-monotonic ψ_s dependence[36]. For precise description of the Stern layer, the layer width and the dielectric profile should be determined by explicit modeling of the molecular interactions between ions, solvent and the surface.

We note that such a successful attempt has been reported in Ref. 37. The Stern layer parameters extracted from molecular dynamic simulations were combined with a PB model and resulted in a quantitative agreement with experiments of the differential capacitance at vanishing surface potential. In contrast to this, non-monotonic ψ_s-dependence of experimental differential capacitance is supposed to be largely due to the ionic profile in the diffuse layer.[6,17,20,21,28]

In our above described model, the Stern layer is not taken into accounted, although, in principle, it can be incorporated by introducing a layer with given thickness and low dielectric constant adjacent to the surface. We leave this refinement to future studies because the main thrust of the present work is to study the interplay between finite ionic size and dielectric decrement, and their effect on ionic profiles and differential capacitance, especially dependence on n_b and ψ_s.

It is experimentally known[38] that the relative permittivity of a bulk electrolyte solution decreases linearly with salt concentration, at low salinity, $n_b \lesssim 2\,\mathrm{M}$. This dependence is written as $\varepsilon = \varepsilon_w - \gamma_b n_b$, where ε_w is the relative permittivity of the solvent (water) and γ_b is a coefficient measured in units of M^{-1}. At higher n_b values, however, the dielectric decrement shows a more complex nonlinear dependence[12,13], which levels off and has a smaller decrement than the linear one.

As we are interested in the EDL behavior where the distribution of counter-ions and co-ions is highly inhomogeneous, we will explicitly take into account the local variation of $\varepsilon(n_{\pm})$ with $n_{\pm}(z)$. Since no direct experiment reported so far the local variation of $\varepsilon(n_{\pm})$ inside the EDL, we will first use a *linear decrement model*, which linearly superimpose the separate contributions of each ionic species[27,28,39]

$$\varepsilon(n_{\pm}) = \varepsilon_w - \gamma_+ n_+(z) - \gamma_- n_-(z)\,, \tag{8}$$

where $\gamma_{\pm}$ is the coefficient of the $\pm$ ion, respectively. These coefficients are not known but can be determined by assuming a simple relationship $\gamma_b = \gamma_+ + \gamma_-$ and using the experimentally known values of γ_b as in Ref. 38. Such values of $\gamma_{\pm}$ are summarized in Table I for several monovalent cations and anions[28,38].

In the numerical calculations presented below (within the linear decrement model of Eq. (8)), we will often use as an example the parameters of a monovalent KCl aqueous solution with $\gamma_{\mathrm{K}^+} = 8\,\mathrm{M}^{-1}$, $a_{\mathrm{K}^+} = 0.662\,\mathrm{nm}$ for K^+, and $\gamma_{\mathrm{Cl}^-} = 3\,\mathrm{M}^{-1}$, $a_{\mathrm{Cl}^-} = 0.664\,\mathrm{nm}$ for Cl^- (see Table I). In addition, the water dielectric constant is $\varepsilon_w = 78.3$ at $T = 25°\mathrm{C}$.

TABLE I. Experimentally obtained coefficients of dielectric decrement[38], γ, and hydration diameter[40], a, for several monovalent cations and anions. The ratio d/a serves as our criterion to determine the mechanism of counter-ion saturation for the linear permittivity decrement (see text). The error bars of γ were reported in Ref. 38 to be about $\pm 1\,\mathrm{M}^{-1}$.

	γ [M^{-1}]	a [nm]	d/a		γ [M^{-1}]	a [nm]	d/a
H^+	17	0.564	1.59	F^-	5	0.704	0.85
Li^+	11	0.764	1.02	Cl^-	3	0.664	0.76
Na^+	8	0.716	0.97	I^-	7	0.662	1.01
K^+	8	0.662	1.05	OH^-	13	0.6	1.37
Rb^+	7	0.658	1.01				

III. STERIC VS. DIELECTROPHORETIC COUNTER-ION SATURATION

At high surface-charge densities, the counter-ions accumulate at the surface due to their strong electrostatic attraction to the oppositely charged surface. However, at some point a saturation concentration is reached as a result of two possible mechanisms: a steric counter-ion saturation or a dielectrophoretic one. The steric effect is due to finite ion size and causes the ionic concentration to saturate at closed packing, estimated as $1/a^3$ where a is the ionic size, while the dielectrophoretic saturation is determined by the coupling between the local dielectric decrement and the ionic profile.

In the high surface-charge limit, we can estimate the concentration at the dielectrophoretic saturation using

the following argument. When the dielectrophoretic saturation is reached before closed packing of the ions, the distance between ions is larger than the inter-ion closest approach and the steric effect can be neglected in Eq. (5), such that $\rho_\pm = n_\pm$. In the counter-ion plateau region, the condition for a counter-ion saturation given by $\partial n_+/\partial z = 0$, leads also to $\partial\epsilon(n_+(z))/\partial z = 0$. Taking the z derivative on both sides of Eq. (6) yields

$$0 = \psi' \left(e - \varepsilon_0 \frac{\partial \varepsilon}{\partial n_+} \psi'' \right) . \tag{9}$$

For large enough $|\sigma|$, the co-ions are almost completely excluded from the EDL, $n_- \approx 0$, and the Poisson equation then becomes

$$\varepsilon_0 \varepsilon_s \psi'' \approx -e n_s^+ , \tag{10}$$

where $n_s^\pm = n_\pm(0)$ are the extrapolated ion concentrations at the surface, and $\varepsilon_s = \varepsilon(n_s^+, n_s^- = 0)$. Combining Eqs. (9) and (10), we define a new function $\Delta\varepsilon_s(n_s^+)$ that should vanish at the saturation condition of n_+,

$$\Delta\varepsilon_s(n_s^+) \equiv \varepsilon_s + n_s^+ \left. \frac{\partial \varepsilon}{\partial n_+} \right|_s = 0 . \tag{11}$$

In order to solve this equation and obtain n_s^+ at dielectrophoretic saturation, an explicit dependence of the permittivity on the counter-ion concentration is required. The simplest model to employ is the linear decrement model introduced in Eq. (8), where $\partial\varepsilon/\partial n_\pm = -\gamma_\pm$. As mentioned above, the linear decrement model is a good approximation for bulk electrolytes of concentration up to about 2 M. Close to the surface, where the counter-ion concentration can be quite high, one needs to consider corrections to linearity as will be presented in Sec. V below.

Returning to the linear decrement case, the above condition, Eq. (11), for dielectrophoretic saturation reduces to

$$\begin{aligned} n_s^+ &= \varepsilon_w/2\gamma_+, \\ \varepsilon_s &= \varepsilon_w/2 . \end{aligned} \tag{12}$$

Note that although a linear decrement is assumed, ε_s at dielectrophoretic saturation does not approach zero for high n_s^+. The limiting values of Eq. (12) are identical to those derived earlier in the salt-free case[27], because even with added salt, the co-ions are taken to be fully depleted from the highly charged surface proximity and do not contribute to the permittivity variation.

A. The generalized Grahame equation

More detailed analysis of counter-ion saturation at the surface can be obtained through the contact theorem or Grahame equation[1,2]. To derive the contact theorem, we first calculate the osmotic pressure from the free energy, Eq. (1)

$$\begin{aligned} P(z) = &- \frac{\varepsilon_0}{2} \left[\varepsilon(n_\pm) + \sum_{\alpha=\pm} n_\alpha \frac{\partial \varepsilon}{\partial n_\alpha} \right] |\psi'|^2 \\ &- \frac{k_B T}{a^3} \ln \phi_w(z) . \end{aligned} \tag{13}$$

At equilibrium, $P(z)$ is a constant independent of z. Equating the pressure at the charged surface $z = 0$, with the pressure in the bulk, $P(\infty)$, gives the modified Grahame equation. Furthermore, when the co-ions are fully depleted from the surface, $n_s^- \to 0$, and we obtain

$$\sigma^2 \simeq \frac{\varepsilon_0 (\varepsilon_s)^2}{\Delta\varepsilon_s} \frac{2 k_B T}{a^3} \ln \left(\frac{\phi_b}{\phi_s} \right) , \tag{14}$$

where $\Delta\varepsilon_s$ was defined in Eq. (11), $\phi_b = 1 - 2a^3 n_b$ and $\phi_s \simeq 1 - a^3 n_s^+$ are, respectively, the solute (water) volume fraction evaluated in the bulk and at the surface. In the linear decrement case, $\Delta\varepsilon_s$ is

$$\Delta\varepsilon_s = \varepsilon_s - \gamma_+ n_s^+ = \varepsilon_w - 2\gamma_+ n_s^+ \tag{15}$$

and the modified Grahame equation reduces to

$$\sigma^2 \simeq \frac{\varepsilon_0 (\varepsilon_w - \gamma_+ n_s^+)^2}{\varepsilon_w - 2\gamma_+ n_s^+} \frac{2 k_B T}{a^3} \ln \left(\frac{\phi_b}{\phi_s} \right) . \tag{16}$$

When the permittivity does not depend at all on the ion concentrations, $\varepsilon(n_\pm) = \varepsilon_w$, the above Grahame equation recovers the sterically-modified Poisson–Boltzmann (smPB) result[19]. It diverges logarithmically at ionic closed-packing, $n_s^+ \to 1/a^3$, which is the maximal value of the ion concentration.

From the generalized Grahame equation (16), it can be seen that the limiting saturation value of n_s^+ is either $\varepsilon_w/2\gamma_+$ for the dielectrophoretic saturation or $1/a^3$ for closed packing. As the surface charge density increases, n_s^+ reaches the smallest value between $\varepsilon_w/2\gamma_+$ and $1/a^3$. To determine which of the two mechanisms prevails, we define an effective size associated with the concentration at dielectrophoretic saturation,

$$d = \left(\frac{2\gamma}{\varepsilon_w} \right)^{1/3} . \tag{17}$$

For ions with $d/a > 1$ the dielectrophoretic saturation prevails, while for ions with $d/a < 1$ the sterically-dominant saturation predominates. This ion-dependent parameter d/a is shown in Table I for several monovalent cations and anions.

As an example, we show in Fig. 1 results for potassium (K^+) ions with the ratio $d/a \simeq 1.05 > 1$, and in Fig. 2 results for chloride (Cl^-) ions with the ratio $d/a \simeq 0.76 < 1$ (ionic parameters are shown in Table I). The (extrapolated) surface value, $n_s^\pm = n_\pm(z \to 0)$, is plotted as function of σ for several values of n_b. For large $|\sigma|$, the

approach of n_s^+ towards the limiting value of $\varepsilon_w/2\gamma_+ \simeq 4.89\,\mathrm{M}$ is clearly observed (Fig. 1 with $d/a > 1$), whereas for $d/a < 1$, n_s^- approaches $1/a^3 \simeq 5.67\,\mathrm{M}$ as σ increases (Fig. 2). In Figs. 1 and 2, we also compare Eq. (16), where co-ions are completely depleted, with the full numerical calculation. Indeed, a very good agreement is observed in the high $|\sigma|$ limit, confirming the applicability of Eq. (16) in this limit, as expected.

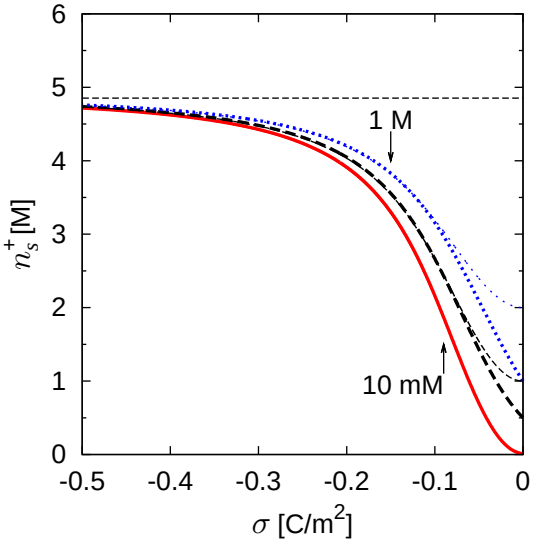

FIG. 1. Dielectrophoretic saturation of counter-ion concentration dominated by the K^+ counter-ions with $d/a \simeq 1.05$. The counter-ion concentration, $n_s^+ = n_+(0)$, at the proximity of a charged surface, is plotted as a function of the negative surface charge density, $\sigma < 0$. The thicker lines are calculated numerically for KCl with bulk values n_b =10 mM (solid red line), 0.5 M (dashed black line) and 1 M (dotted blue line). The K^+ and Cl^- parameters are shown in Table I, $T = 25^\circ$ C and $\varepsilon_w = 78.3$. The thinner blue and black lines are the analytical approximated n_s^+ obtained from the Grahame equation (16) with the same bulk values of n_b, respectively, as for the thick lines, and by setting $n_s^- = 0$. Note that for the red line of 10 mM, the analytical line is indistinguishable from the numerical one. The concentration at the dielectrophoretic saturation, $\varepsilon_w/2\gamma_{K^+} \simeq 4.89\,\mathrm{M}$, is indicated by a horizontal dashed line.

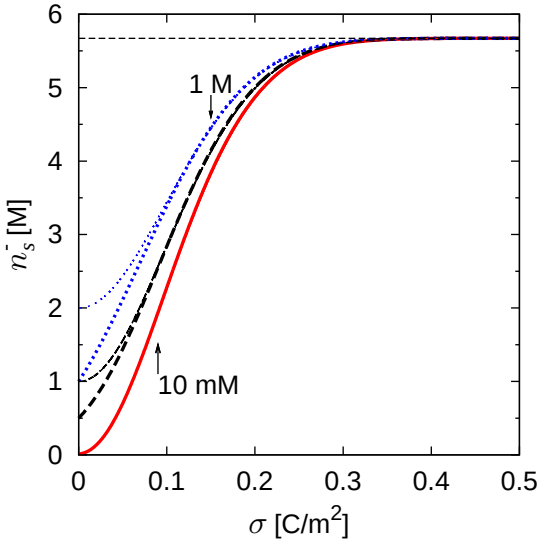

FIG. 2. Sterical saturation of counter-ion concentration dominated by Cl^- counter-ions with $d/a \simeq 0.76$. The counter-ion concentration, $n_s^- = n_-(0)$, at the proximity of a charged surface, is plotted as a function of the positive surface charge density, $\sigma > 0$. The thicker lines are calculated numerically for KCl with bulk values n_b =10 mM (solid red line), 0.5 M (dashed black line) and 1 M (dotted blue line). The K^+ and Cl^- parameters are shown in Table I, $T = 25^\circ$ C and $\varepsilon_w = 78.3$. The thinner lines are the approximate n_s^- as obtained from the Grahame equation (16) with the same n_b bulk values, respectively, and by setting $n_s^+ = 0$. Note that for the red line of 10 mM, the analytical line is indistinguishable from the numerical one. The concentration at closed packing, $1/a_{Cl^-}^3 \simeq 5.67\,\mathrm{M}$, is indicated by a horizontal dashed line.

IV. DIFFERENTIAL CAPACITANCE

Irrespective of the underlying mechanism, when counter-ion saturation occurs, the EDL width will grow. This effect can be shown by considering the *differential capacitance*, $C(\psi_s) = \partial\sigma/\partial\psi_s$.

We derive an analytic expression for C under the assumption that co-ions are fully depleted from the surface, $n_s^- = 0$. As was shown earlier this gives a simplified expression for the surface permittivity, $\varepsilon_s \simeq \varepsilon_w - \gamma_+ n_s^+$ and $\Delta\varepsilon_s \simeq \varepsilon_w - 2\gamma_+ n_s^+$. The results are presented here within the linear decrement model, and later (Sec. V) they will be generalized to the non-linear case. The relation between ψ_s and n_s^+ is obtained from the equilibrium distribution, Eqs. (5) and (6), at the surface by eliminating ψ' with $\sigma(n_s^+)$ from Eq. (16) and the boundary condition, Eq. (7), and $\rho_s^+ = n_s^+(\phi_b/\phi_s)$

$$\Psi_s = \ln\left(\frac{n_b}{n_s^+}\right) - \frac{\Delta\varepsilon_s + \gamma_+ a^{-3}}{\Delta\varepsilon_s} \ln\left(\frac{\phi_b}{\phi_s}\right) . \qquad (18)$$

where $\Psi_s \equiv e\psi_s/k_BT$ is the dimensionless surface potential to be used hereafter. Next, the differential capacitance is obtained as the parametric function of n_s^+:

$$C = \frac{e}{k_BT}\frac{\partial\sigma}{\partial n_s^+}\left(\frac{\partial\Psi_s}{\partial n_s^+}\right)^{-1} , \qquad (19)$$

where

$$\frac{\partial\Psi_s}{\partial n_s^+} = -\frac{1}{n_s^+} - \frac{\Delta\varepsilon_s + \gamma_+ a^{-3}}{\Delta\varepsilon_s}\left(\frac{a^3}{\phi_s}\right)$$

$$- \frac{2\gamma_+^2}{a^3\left(\Delta\varepsilon_s\right)^2} \ln\left(\frac{\phi_b}{\phi_s}\right) , \qquad (20)$$

and

$$\frac{\partial\sigma}{\partial n_s^+} = \frac{1}{\Delta\varepsilon_s}\left(\frac{k_B T\varepsilon_0\varepsilon_s^2}{\phi_s\sigma} + \frac{\sigma n_s^+\gamma_+^2}{\varepsilon_s}\right), \qquad (21)$$

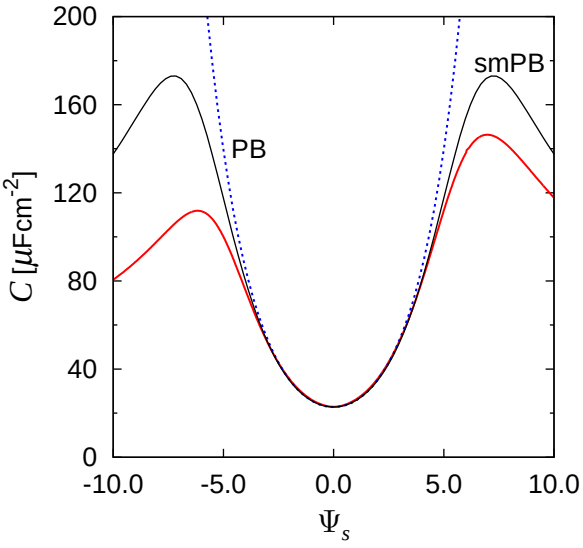

FIG. 3. Comparison of the differential capacitance C calculated for KCl (parameters as in Table I) with $n_b = 10\,\mathrm{mM}$. The red solid line corresponds to the exact numerical solution, the blue dotted line is the regular PB result, Eq. (22), and the black solid line is the smPB result, Eq. (23). The peaks of the red curves are located at $\Psi_s = 6.98$ and $\Psi_s = -6.15$, and those of the black curves are at $\Psi_s = \pm 7.25$.

Figures 3 and 4 shows the numerically-calculated C as a function of Ψ_s for KCl concentration $n_b = 10\,\mathrm{mM}$, along with several analytic results. At this salt concentration, the calculated C shows two peaks, one for $\Psi_s < 0$ and the other for $\Psi_s > 0$. This characteristic shape of the differential capacitance is called *camel-shape* or *double-hump*[20], and is often observed in experimental differential capacitance[14–16,36] at relatively low salt concentrations. It is quite different from the well-known capacitance of the standard PB model, C_{PB}, which is obtained in our model by setting $\gamma_\pm = a = 0$,

$$C_{\mathrm{PB}} = \varepsilon_0\varepsilon_w\lambda_D^{-1}\cosh(\Psi_s/2)\,, \qquad (22)$$

where $\lambda_D = \sqrt{\varepsilon_0\varepsilon_w k_B T/2n_b e^2}$ is the Debye-Hückel screening length. The PB capacitance is applicable to small surface potentials, and has a minimum at $\Psi_s = 0$. However, as is seen in Fig. 3, it does not reproduce the two peaks for larger $|\Psi_s|$. In contrast, the capacitance calculated from the analytical expressions, Eqs. (18)-(21), is found to reproduce well the full (numerical) dependence of $C(\Psi_s)$, including the two asymmetric peaks in C (Fig. 4). A deviation of this analytical expression from the numerical one is noticed at small values of the

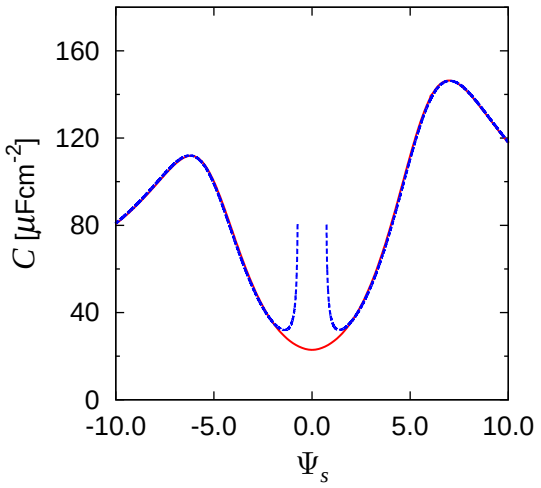

FIG. 4. Comparison of the analytic differential capacitance C with the numerical one calculated for KCl (parameters as in Table I) with $n_b = 10\,\mathrm{mM}$. The red solid line (just as in Fig. 3) corresponds to the full numerical solution, while the blue dashed line denotes the approximate analytic expression of Eqs. (18)-(21). The analytical results reproduce the numerical ones in all range of $|\Psi_s| \gtrsim 2$, including the two asymmetric peak heights at $\Psi_s = 6.98$ and $\Psi_s = -6.15$, while C_{PB} reproduces well the C behavior for small $|\Psi_s| \lesssim 2$.

potential, $|\Psi_s| \lesssim 2$, and C from Eqs. (18)-(21) even diverges for $|\Psi_s| \to 0$, because the assumption that co-ions are fully depleted from the surface is not valid anymore.

It is possible to describe the full dependence of $C = C(\Psi_s)$ by two analytical expressions: (i) C_{PB} of Eq. (22) for small Ψ_s, and (ii) the expression of Eqs. (18)-(21) for large Ψ_s. Using the approximate two-patch expressions for C, we can reproduce a line that is almost indistinguishable from the red line of Fig. 4, which was obtained numerically from the full expression. The crossover between the two regions occurs at about the same Ψ_s where C (derived from Eqs. (18)-(21)) starts to sharply increase above C_{PB}. Below the crossover Ψ_s, the co-ion concentration at the surface, n_s^-, becomes significant. As n_s^- reduces the capacitance, Eqs. (18)-(21) that *do not* include their presence, start to deviate sharply from the behavior describes by C_{PB}.

We note that the two peaks at the two surface-polarities, $\Psi_s \lessgtr 0$, have different origins resulting in non-equal peak heights. The build-up of the EDL is dominated by the cations for $\Psi_s < 0$ and by the anions for $\Psi_s > 0$. In the particular example for KCl (Fig. 3), K^+ is the counter-ion for $\Psi_s < 0$ with $d/a > 1$ (dielectrophoretic-dominant case), while Cl^- is the counter-ion for $\Psi_s > 0$ with $d/a < 1$ (sterically-dominant case), and this explains the asymmetry of the two peaks.

In order to check the effect of dielectric decrement, we also plot in Fig. 3 the analytic differential capacitance

for the smPB model, $C_{\rm smPB}$, which was derived previously[20,21]

$$C_{\rm smPB} = \frac{C_{\rm PB}}{1+4a^3 n_b \sinh^2(\Psi_s/2)} \times \sqrt{\frac{4a^3 n_b \sinh^2(\Psi_s/2)}{\ln\left(1+4a^3 n_b \sinh^2(\Psi_s/2)\right)}}\,, \qquad (23)$$

The peak position within the smPB model can be roughly estimated[21,41] by substituting the closed-packing concentration, $n_s = 1/a^3$ into the Boltzmann distribution, $n_s^{\pm} = n_b \exp(\mp\Psi^{\rm str})$, yielding $|\Psi^{\rm str}| \simeq -\ln(a^3 n_b)$. For the case of Fig. 3, it gives $|\Psi^{\rm str}| \simeq 6.34$ with $a_{\rm Cl^-} = 0.664\,$nm. Although $C_{\rm smPB}$ also exhibits double-hump shape, the peak positions (in Ψ_s) and their corresponding heights differ from the ones in our model, as will be discussed in detail in the subsequent sections.

For KCl with n_b =10 mM as in Fig. 3, C at $\Psi_s = 0$ is 22.9 μFcm^{-2}, and it overestimates typical experimental data[37]. This discrepancy is probably due to the omission of the Stern layer. For quantitative description of experimental differential capacitance, appropriate modeling of the Stern layer is required in addition to the EDL.

From the differential capacitance, we can estimate the EDL width as

$$l(n_b, \sigma(\psi_s)) = \varepsilon_0 \varepsilon_s / C\,. \qquad (24)$$

In Fig. 5, l is plotted as a function of Ψ_s for several values of n_b. For small n_b (n_b = 10 mM in Fig. 5), l first decreases with $|\Psi_s|$ due to the increasing electrostatic attraction between the surface and the counter-ions. Note that the regular PB theory is valid for such small $|\Psi_s|$, and gives similar results. For larger $|\Psi_s|$, after saturation of the counter-ion concentration is reached, l starts to increase with $|\Psi_s|$ as n_s reached saturation and the accumulated counter-ions contribute to thickening the EDL.

As n_b increases (n_b = 0.1 M in Fig. 5), n_s can reach saturation at even smaller $|\Psi_s|$, and the range of Ψ_s where the PB theory can be applied diminishes. When n_b increases even further (n_b = 1 M in Fig. 5), n_s immediately reaches saturation even for small applied Ψ_s. Therefore, the increase of l with $|\Psi_s|$ already starts from $\Psi_s = 0$. In this high salinity range, the regular PB theory cannot be applied at all. The crossover from low- to high-salinity will be further discussed in Sec. IV C.

A. The dielectrophoretic saturation for $d > a$

For the case of KCl in contact with a negatively charged surface, the counter-ion is K^+ (potassium) with $d/a > 1$, where d has been already defined in Eq. (17) as the effective size at the dielectrophoretic saturation concentration. The EDL of this counter-ion exhibits a dielectrophoretic saturation. The location of the peak in C, $\Psi^{\rm die} < 0$, can be estimated similarly to the way

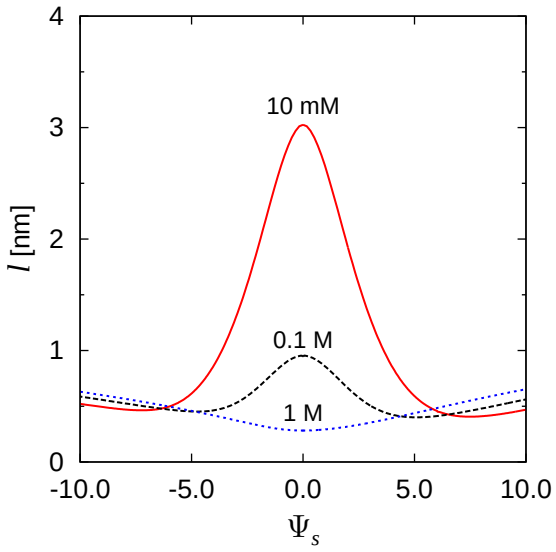

FIG. 5. The width of the electric double layer estimated from the differential capacitance, $l = \varepsilon_0\varepsilon_s/C$, as a function of dimensionless surface potential, Ψ_s, for KCl (parameters as in Table I) with n_b =10 mM (solid red line), 0.1 M (dashed black line) and 1 M (dotted blue line).

$\Psi^{\rm str}$ was estimated after Eq. (23) above. We substitute $n_s^+ = \varepsilon_w/2\gamma_+$ into the Boltzmann distribution, and obtain $\Psi^{\rm die} = e\psi^{\rm die}/k_BT \simeq -\ln(\varepsilon_w/2\gamma_+ n_b)$. For the case in Fig. 3, this estimation gives $\Psi^{\rm die} \simeq -6.19$.

For ions with $d/a > 1$, the threshold surface potential for dielectrophoretic counter-ion saturation is smaller than that for steric saturation. Namely, $|\Psi^{\rm die}| < |\Psi^{\rm str}|$, and the peak in C originates from the dielectrophoretic counter-ion saturation. In Fig. 6, we plot the K^+ counter-ion profile, $n_+(z)$, and the corresponding permittivity variation, $\varepsilon(z)$, as function of the distance z from the surface, for n_b = 10 mM. For this case[27,28] with $d/a > 1$, n_s^+ approaches the concentration at the dielectrophoretic saturation, which is smaller than the closed-packing concentration, $\varepsilon_w/2\gamma_+ < 1/a^3$ (see Fig. 6(a)).

For comparison, the results of the regular PB model ($a = 0$), which, nevertheless, includes the dielectrophoretic effect via $\varepsilon(n(z))$, are also plotted in Fig. 6 (dotted blue line). The steric effect slightly suppresses the concentration near the surface, but the width of the diffuse layer is almost unaffected. The surface permittivity ε_s approaches $\varepsilon_w/2$, which is half that of the bulk. Hence, the differential capacitance for counter-ions with $d/a > 1$ is considerably lower than that derived for the smPB model. In Fig. 3, the C-value at the $\Psi_s < 0$ peak of the full model is 111.9 μFcm^{-2}, while that of the smPB is 173.1 μFcm^{-2}.

For $|\Psi_s| > |\Psi^{\rm die}|$, the differential capacitance starts to decrease due to the increasing EDL width, l. At very high surface potentials, $|\Psi_s| \gg |\Psi^{\rm die}|$, the asymptotic form of the differential capacitance for the dielectrophoretic

saturation can be derived from Eqs. (20)-(21):

$$C^{\infty}_{\rm die} \simeq \sqrt{\frac{\varepsilon_0\varepsilon_w e^2}{4d^3 k_B T}}\,\frac{1}{\sqrt{|\Psi_s| + \ln\left(d^3 n_b\right)}}\,, \qquad (25)$$

The inverse-square-root decay of C is similar to that observed in the sterically-dominant saturation[20,21], but with the difference that the effective size d replaces a, and the limiting surface permittivity $\varepsilon_s = \varepsilon_w/2$ replaces ε_w.

As a conclusion of the above discussion we would like to state that for ions with $d/a > 1$, the stronger mechanism is the dielectric decrement, and the peak positions of the differential capacitance occur at lower values of $|\Psi_s|$ than for the smPB model. The peak heights in C are reduced because of the dielectrophoretic saturation and corresponding reduction of the surface permittivity.

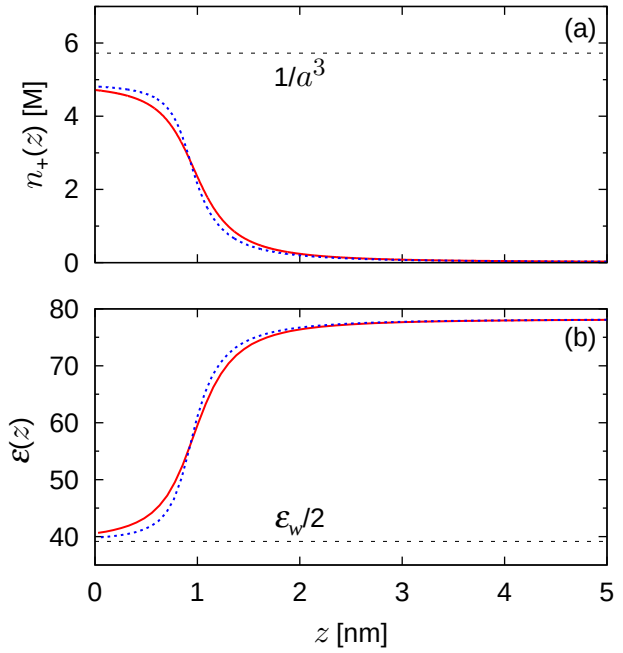

FIG. 6. (a) Counter-ion density profile, $n_+(z)$, as function of the distance z from a negatively charged surface with $\sigma = -0.5\,\mathrm{C/m^2}$, for KCl concentration $n_b = 10\,\mathrm{mM}$ (red solid line). The K^+ values of a and d are taken from Table I. The dotted (blue) line represents the profile of the regular PB that includes the dielectrophoretic effect, $\varepsilon = \varepsilon(n(z))$, but without the steric effect ($a = 0$). The dashed (black) line corresponds to closed-packing concentration $1/a^3 = 5.72\,\mathrm{M}$ for K^+, and is bigger than the actual saturation concentration here. (b) The relative permittivity profile, $\varepsilon(z)$ (red solid line). The dotted blue line represents the profile of the regular PB that includes the dielectrophoretic effect. The dashed line corresponds to the permittivity at the limiting dielectrophoretic saturation, $\varepsilon_s = \varepsilon_w/2$.

B. The sterically-dominant saturation for $d < a$

For ions with $d/a < 1$, the hydration size, a, is larger than the effective size at dielectrophoretic saturation, d, the magnitude of the threshold surface potential is smaller for the sterically-dominant saturation of counter-ion concentration than for the dielectrophoretic one. Namely, $|\Psi^{\rm str}| < \left|\Psi^{\rm die}\right|$, and the peak in C originates from the sterically-dominant counter-ion saturation. This is seen for large values of $\Psi_s > 0$ in Fig. 3, where the behavior in C is dominated by the Cl^- counter-ion with $d/a < 1$, and the EDL exhibits the sterically-dominant counter-ion saturation (Fig. 2).

In Fig. 7, we plot the Cl^- counter-ion profile, $n_-(z)$, and the corresponding permittivity variation, $\varepsilon(z)$, for $n_b = 10\,\mathrm{mM}$. At the surface, n_s^- reaches the closed-packing value of $1/a^3$, because the latter is smaller than the dielectrophoretic value, $1/a^3 < \varepsilon_w/2\gamma_-$. For comparison, the results of the smPB model with $\gamma_\pm = 0$ are also calculated. However, it turns out that the ion density profiles with or without $\gamma_\pm$ are almost identical (and their slight difference is below the resolution of the figure). As the Cl^- concentration is below the concentration at the dielectrophoretic saturation for $d/a < 1$, the dielectric decrement is smaller (Fig. 7(b)), as compared with the K^+ case of Fig. 6(b).

Although the counter-ion concentration, $n_-(z)$, is barely affected by the dielectric decrement, the smPB model overestimates the peak position (in Ψ_s) and the height of C (Fig. 3). The dielectric decrement in the diffuse layer (with ε decreasing from 78.3 to about 61.3) is not so large, but the effect of dielectric decrement prevails even for $d/a < 1$. For the sterically-dominant saturation, the asymptotic expression for $|\Psi_s| \gg |\Psi^{\rm str}|$ can be derived from Eqs. (20)-(21):

$$C^{\infty}_{\rm str} \simeq \sqrt{\frac{e^2}{2a^3 k_B T}}\sqrt{\frac{\varepsilon_0\left(\varepsilon_w - \gamma_-/a^3\right)}{|\Psi_s| + \ln(a^3 n_b)}}\,. \qquad (26)$$

In comparison[20,21], the asymptotic expression of $C_{\rm smPB}$ from Eq. (23) is just like Eq. (26) but with $\gamma_- = 0$. As compared to the smPB model, $C^{\infty}_{\rm str}$ is reduced by the effect of the permittivity decrement at the surface, $\varepsilon_s < \varepsilon_w$.

C. Crossover from camel-shape to bell-shape at high salt

As the salt concentration n_b increases, the threshold in $|\Psi_s|$ either for the dielectrophoretic saturation, $\left|\Psi^{\rm die}\right|$, or for the sterically-dominant saturation, $|\Psi^{\rm str}|$, decreases and the position of the two peaks in C approaches $\Psi_s = 0$. Simultaneously, the differential capacitance at $\Psi_s = 0$, estimated as $C(0) \approx C_{\rm PB}(0) = \varepsilon_0\varepsilon_w/\lambda_D$, increases as n_b increases, until at some value of n_b, C becomes uni-modal (bell shape) with a single peak at $\Psi_s \approx 0$. Clearly that for these high salinity conditions, the standard PB is not valid even for small Ψ_s.

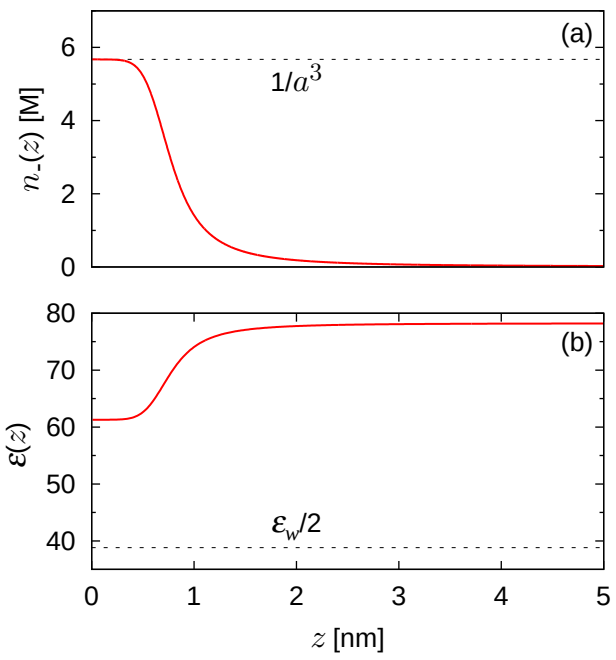

FIG. 7. (a) Counter-ion density profile, $n_-(z)$, as function of the distance z from a positively charged surface, $\sigma = 0.5\,\mathrm{C/m^2}$, for KCl concentration $n_b = 10\,\mathrm{mM}$ (red solid line). The Cl^- values of a and d are taken from Table I. The dashed line corresponds to closed-packing concentration for Cl^-, $n_s^- = 1/a^3 \simeq 5.67\,\mathrm{M}$. (b) Corresponding permittivity profile, $\varepsilon(z)$ (red solid line). The dashed line corresponds to the permittivity at the limiting dielectrophoretic saturation, $\varepsilon_w/2$.

We would like to get an estimation for n_b at the crossover from camel-shape to bell-shape. At this n_b^* value, the differential capacitance at $\Psi_s = 0$ becomes comparable to the lower of the two peaks (located at $\Psi_s \lessgtr 0$). The C-values at the two peaks can be roughly estimated by using the expression of $C_{\rm PB}$ of Eq. (22), where ε_w in $C_{\rm PB}$ is replaced with ε_s:

$$C(\Psi_s) = \sqrt{\frac{2\varepsilon_0\varepsilon_s e^2 n_b}{k_B T}}\cosh(\Psi_s/2)\,. \tag{27}$$

For ions with $d/a > 1$ where the dielectrophoretic saturation is dominant, C at the peak is estimated by substituting $|\Psi^{\rm die}| \simeq \ln(\varepsilon_w/2\gamma n_b)$ and $\varepsilon_s = \varepsilon_w/2$ into Eq. (27)

$$C(\Psi^{\rm die}) \simeq \frac{C(0)}{\sqrt{8}}\sqrt{\frac{\varepsilon_w}{2\gamma n_b}}\,. \tag{28}$$

Namely, for ions with $d/a > 1$ the crossover is expected to occur around $n_b^* \simeq \varepsilon_w/16\gamma$, and for K^+ it gives $n_b^* \simeq 0.61\,\mathrm{M}$.

For the other case of ions with $d/a < 1$, where the steric saturation is dominant, C at the peak is estimated by substituting $\Psi^{\rm str} \simeq -\ln(a^3 n_b)$ and $\varepsilon_s = \varepsilon_w - \gamma/a^3$ into the C expression from Eq. (27)

$$C(\Psi^{\rm str}) \simeq C(0)\sqrt{\frac{2-(d/a)^3}{8a^3 n_b}}\,. \tag{29}$$

and the crossover salt concentration occurs at:

$$n_b^* \simeq \frac{2-(d/a)^3}{8a^3}\,. \tag{30}$$

For Cl^-, this salt concentration is estimated to be $n_b^* \simeq 1.1\,\mathrm{M}$. Therefore, combining the results for K^+ and Cl^-, we find that the crossover from camel-shape to bell-shape for KCl is expected at the smallest of the n_b^* estimates for K^+ and Cl^-. And in our case, $n_b^* \lesssim 0.61\,\mathrm{M}$.

In Fig. 8, the numerically calculated C for KCl concentration of $n_b = 0.1\,\mathrm{M}$ and $1\,\mathrm{M}$ is plotted. For the lower salt concentration of $0.1\,\mathrm{M}$, a double-hump C is observed, while for the higher salt concentration of $1\,\mathrm{M}$, C becomes uni-modal, as the two peaks merge together. We remark that for the smPB model, the uni-modal (bell-shape) differential capacitance has been already derived in Ref. 20, while in the present work the changeover from double-hump to bell-shape capacitance is investigated, by considering the combined ion finite-size and dielectric decrement effects. The value of n_b^* at the crossover, as obtained from our numerical calculations, is about $0.6\,\mathrm{M}$, which is comparable to n_b^* estimated above.

For high salinity, the bell-shaped C is skewed and its peak is located at slightly positive surface potential, $\Psi_s \gtrsim 0$ (Fig. 8 with $n_b = 1\,\mathrm{M}$), in contrast to lower salt concentration, where the minimum in C always occurs at $\Psi_s = 0$. When the bell-shaped C occurs at high n_b, the EDL width increases with $|\Psi_s|$. Consequently, it always contributes to a decrease in C as $|\Psi_s|$ increases, because of the relation, $C = \varepsilon_0\varepsilon_s/l$. Accordingly, the increase of C implies an increase of ε_s with $|\Psi_s|$.

In Fig. 9, ε_s is plotted as a function of Ψ_s. The figure clearly shows that for $\Psi_s > 0$, ε_s first increases from $\Psi_s = 0$, then has a peak at small and finite Ψ_s, and afterwards it decreases. From this observation, we assert that the peak of the bell-shaped C originates from the increase of ε_s for small $\Psi_s > 0$. When finite $|\Psi_s|$ is applied, an EDL develops and the counter-ion n_s increases. However, it does not always mean that ε_s decreases with $|\Psi_s|$. With the built-up of EDL, n_s of the co-ions decreases, which contribute to *increasing* ε_s from the value $\epsilon_w - (\gamma_+ + \gamma_-)n_b$ at $\Psi_s = 0$. To understand the observed non-monotonic change of ε_s with $\Psi_s > 0$, the asymmetry of $\gamma_\pm$ should be considered, in addition to the ionic concentration change between the bulk and the surface, $n_s^\pm - n_b$.

For the specific case of KCl, $\gamma_{K^+} > \gamma_{Cl^-}$, and for $\Psi_s > 0$, the contribution from the K^+ co-ions dominates over that of the Cl^- counter-ions, resulting in a net increase of ε_s as in Fig. 9. This phenomenon is more prominent for higher n_b, because $\varepsilon_s(\Psi_s = 0)$ is further reduced, leading to a more substantial permittivity increase due to the decrease in the K^+ co-ion concentration (Fig. 9).

In summary, the non-monotonic dependence of ε_s on $|\Psi_s|$ is expected to occur when the dielectric decrement of the co-ions is larger than that of the counter-ions, $\gamma_{K^+} > \gamma_{Cl^-}$. At high salt concentrations, when the PB model becomes invalid at any surface potential, this effect leads to a skewed bell-shape differential capacitance, and the occurrence of the peak of bell-shaped C at $\Psi_s \neq 0$.

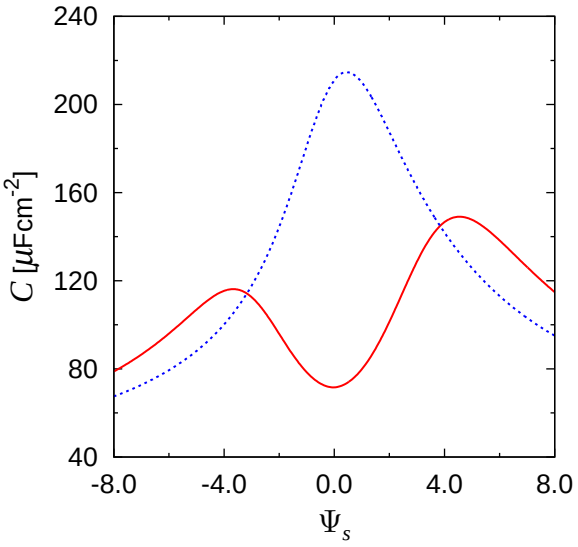

FIG. 8. Differential capacitance C as a function of dimensionless surface potential, Ψ_s, calculated for KCl (parameters in Table I). For $n_b = 0.1$ M (red solid line) C exhibits a double-humped camel-shape, while for $n_b = 1$ M (blue dotted line) it exhibits skewed bell-shape. The peaks of the red line are located at $\Psi_s = 4.56$ and $\Psi_s = -3.67$, while the peak of the uni-modal C occurs at $\Psi_s = 0.46$.

V. EFFECTS OF NONLINEAR DECREMENT

The linear decrement model[38] is a good approximation for salt concentrations up to about, $n_b \lesssim 2$M. Close to the surface, where the counter-ion concentration is high, nonlinear dependence on the counter-ion concentration is expected and the permittivity decrement usually becomes weaker than for the linear decrement. Because there are no direct experiments that reported the local variation of $\varepsilon(n_\pm)$ inside the EDL, we investigate the effect of nonlinear decrement by comparing several available models.

A. Effect of quadratic term in $\varepsilon(n)$

To study the effect of nonlinear correction to the permittivity decrement, we expand the permittivity up to

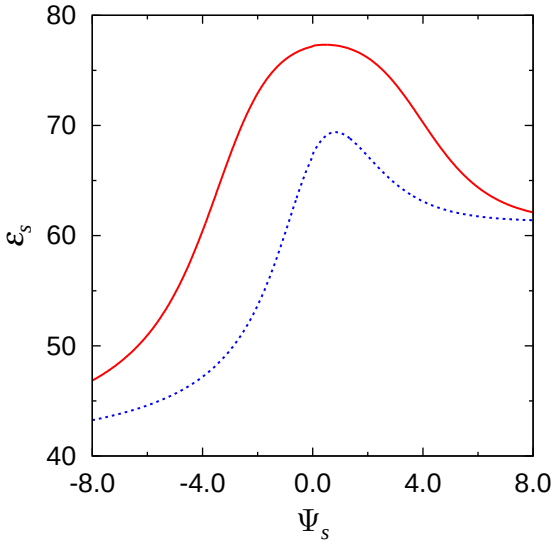

FIG. 9. Surface permittivity, ε_s, as a function of the dimensionless surface potential, Ψ_s, for KCl (parameters in Table I). The solid (red) line corresponds to $n_b = 0.1$ M, with a peak at $\Psi_s = 0.46$, while the dotted (blue) line corresponds to $n_b = 1$ M, with a peak at $\Psi_s = 0.81$.

second order in $n_\pm$

$$\varepsilon(n_\pm) = \varepsilon_w - \sum_{\alpha=\pm}\left(\gamma_\alpha n_\alpha(z) - \frac{1}{2}\beta_\alpha n_\alpha^2\right), \qquad (31)$$

with $\gamma_\pm = -\partial\varepsilon/\partial n_\pm|_s$ as before and $\beta_\pm = \partial^2\varepsilon/\partial n_\pm^2|_s$, evaluated at the same $z = 0$ surface. Because the bulk permittivity, $\varepsilon(n_b)$, is known from experiments to be a concave function[12,13,42,43], we assume $\beta_\pm \geq 0$.

Analytical results can be obtained as before with the assumption that the co-ions are completely depleted from the negatively charged surface, $n_s^- \to 0$. This is a very good approximation as long as $|\Psi_s|$ is not too small. Using it we get

$$\varepsilon_s \simeq \varepsilon_w - \gamma_+ n_s^+ + \frac{1}{2}\beta_+ (n_s^+)^2 . \qquad (32)$$

We define (as before) a related surface permittivity $\Delta\varepsilon_s$ as:

$$\begin{aligned}\Delta\varepsilon_s &= \varepsilon_s + n_s^+ \left.\frac{\partial\varepsilon}{\partial n_+}\right|_s \\ &= \varepsilon_w - 2\gamma_+ n_s^+ + \frac{3}{2}\beta_+ (n_s^+)^2 \\ &= \varepsilon_s - \gamma_+ n_s^+ + \beta_+ (n_s^+)^2 . \end{aligned} \qquad (33)$$

From the osmotic pressure expression, Eq. (13), it is easy to derive the modified Grahame equation[1,2] as applied to the non-linear $\varepsilon(n_\pm)$:

$$\sigma^2 \simeq \frac{\varepsilon_0 (\varepsilon_s)^2}{\Delta\varepsilon_s}\frac{2k_B T}{a^3}\ln\left(\frac{\phi_b}{\phi_s}\right) . \qquad (34)$$

Note that it has exactly the same form as Eq. (16) (the linear decrement), but with different ε_s and $\Delta\varepsilon_s$ as in Eqs. (32)-(33) for the non-linear case.

The differential capacitance C also depends on β_+. It is obtained as the parametric function of n_s^+, (just as in Eq. (19)), where

$$\Psi_s = \ln\left(\frac{n_b}{n_s^+}\right) - \frac{\Delta\varepsilon_s + (\gamma_+ - \beta_+ n_s^+)\, a^{-3}}{\Delta\varepsilon_s} \ln\left(\frac{\phi_b}{\phi_s}\right) . \tag{35}$$

and

$$\frac{\partial \Psi_s}{\partial n_s^+} = -\frac{1}{n_s^+} - \frac{\Delta\varepsilon_s + (\gamma_+ - \beta_+ n_s^+)\, a^{-3}}{\Delta\varepsilon_s}\left(\frac{a^3}{\phi_s}\right) + \frac{\varepsilon_s\beta_+ - 2\left(\gamma_+ - \beta_+ n_s^+\right)^2}{a^3(\Delta\varepsilon_s)^2} \ln\left(\frac{\phi_b}{\phi_s}\right) , \tag{36}$$

$$\frac{\partial \sigma}{\partial n_s^+} = \frac{k_B T}{\sigma\phi_s}\frac{\varepsilon_0\varepsilon_s^2}{\Delta\varepsilon_s} + \frac{\sigma n_s^+}{2\varepsilon_s\Delta\varepsilon_s}\left[2\left(\gamma_+ - \beta_+ n_s^+\right)^2 - \varepsilon_s\beta_+\right] , \tag{37}$$

Nonlinear correction of the permittivity decrement at high counter-ion concentration implies that the concentration at the dielectrophoretic saturation should change, as is clearly seen from the modified Grahame equation, Eq. (34). By solving Eq. (33) with non-zero $\beta_+ > 0$, the concentration at dielectrophoretic saturation becomes

$$n_s^+ = \frac{2\gamma_+ - 2\sqrt{\gamma_+^2 - 3\beta_+\varepsilon_w/2}}{3\beta_+} \simeq \frac{\varepsilon_w}{2\gamma_+}\left(1 + \frac{3\beta_+\varepsilon_w}{8\gamma_+^2}\right) , \tag{38}$$

where we assume that the quadratic term represents a small correction, $0 < \beta_+ \ll 2\gamma_+^2/3\varepsilon_w$. It shows that the dielectrophoretic saturation concentration shifts to higher values of n_s^+ as compared with those predicted by the linear decrement. The effective size of the dielectrophoretic saturation for the nonlinear decrement (denoted as $d^{\rm NL}$) becomes smaller than that of the linear decrement, $d^{\rm NL} < d$.

In Fig. 10, we plot n_s^+ at dielectrophoretic saturation for K^+ ions, as a function of the quadratic coefficient, β_+. The figure shows that n_s^+ at the dielectrophoretic saturation increases with β_+. Moreover, when the quadratic coefficient is considerably large, $\beta_+ > 2\gamma_+^2/3\varepsilon_w$, the dielectrophoretic saturation does not occur, and $d^{\rm NL} \to 0$ in this extreme case. The increase of the dielectrophoretic saturation concentration implies a possible change of the working saturation mechanism towards the sterically-dominant one. For the K^+ ions, the dielectrophoretic saturation is predicted for the linear decrement model because $d/a > 1$ (see Table I). This can also be observed for $\beta_+ = 0$ in Fig. 10. The change of the saturation mechanism occurs for $\beta_+ \gtrsim 0.27$, where $n_s^+ \gtrsim 1/a^3$ and the condition $d^{\rm NL}/a < 1$ is satisfied.

In general, weakening the permittivity decrement ($\beta^+ > 0$) at higher ion concentration increases the value of n_s^+ at the dielectrophoretic saturation, and may even lead to disappearance of this saturation. The latter scenario depends on the specific type of the nonlinear decrement model as will be demonstrated next.

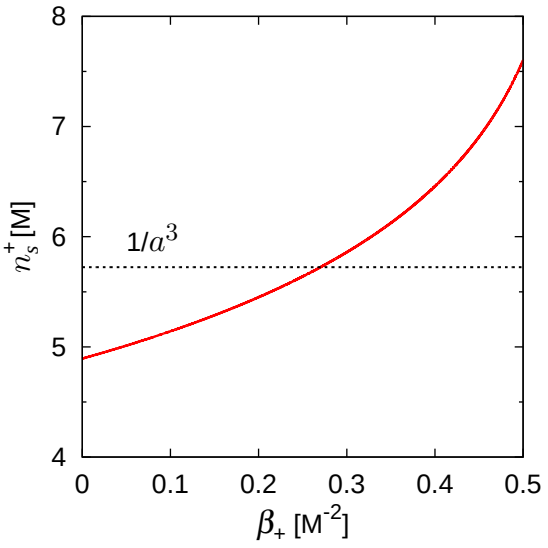

FIG. 10. The concentration at the dielectrophoretic saturation for the quadratic permittivity model, Eq. (32), as a function of the quadratic coefficient, β_+. The parameters are $\varepsilon_w = 78.3$ and $\gamma_+ = 8$ (K^+ ions). The dotted line indicates the closed-packing concentration for the K^+ ions.

B. Non-linear $\varepsilon(n)$ of a one-loop expansion

An analytic expression for bulk permittivity of electrolyte solutions has been derived in Refs. 12 and 13 using the dipolar Poisson–Boltzmann (DPB) model. The free energy of the electrolyte solution takes into account the ionic and dipolar degrees of freedom. The field-theoretical calculation employs a one-loop expansion of the free energy beyond mean-field theory, and accounts for the fluctuations in ion and dipolar solvent concentra-

tions. At high salinity, the permittivity function, $\varepsilon(n_b)$, has a nonlinear dependence on the salt concentration n_b, and fits nicely experiments that also observed nonlinear behavior of $\varepsilon(n_b)$ in that high salt range. The ionic solution permittivity $\varepsilon(n_b)$ was found to be:

$$\begin{aligned}\varepsilon_w &= \varepsilon_{\rm DPB} + \frac{(\varepsilon_{\rm DPB}-\varepsilon_0)^2}{\varepsilon_{\rm DPB}}\frac{4\pi}{3c_d b^3}\,,\\ \varepsilon_{\rm DPB} &= \varepsilon_0 + \frac{p_0^2 c_d}{3k_B T},\\ \varepsilon(n_b) &= \varepsilon_w \\ &\quad - \frac{(\varepsilon_{\rm DPB}-\varepsilon_0)^2}{\varepsilon_{\rm DPB}}\frac{\kappa_D^2}{\pi c_d b}\left(1-\frac{\kappa_D b}{2\pi}\tan^{-1}\frac{2\pi}{\kappa_D b}\right),\end{aligned} \tag{39}$$

where $p_0 = 1.8\,{\rm D}$ is the water dipolar moment, $c_d = 55\,{\rm M}$ is the water molar density, $\kappa_D = \sqrt{8\pi l_B n_b}$ is the inverse Debye-Hückel length, $l_B = e^2/(4\pi\varepsilon_{\rm DPB}k_B T)$ is the Bjerrum length, $T = 300$ K, and b is the microscopic cutoff length. The latter incorporates into its value the distance of closest approach between all types of ions and dipoles, and is used as a fitting parameter to experimental results. Note that in the DPB model, ε_w of Eq. (39) is a function of the water dipolar moment (p_0) and density (c_d). The permittivity of the ionic solution, $\varepsilon(n_b)$, depends in addition on the ions and their interactions with the dipoles.

Because we are interested in the EDL behavior, we need to extract the explicit dependence of ε on the local counter-ion and co-ion concentrations, $n_\pm(z)$. The permittivity of Eq. (39) depends on n_b through κ_D. As it is difficult to separate the contributions from cations and anions in Eq. (39), we replace n_b with $(n_+ + n_-)/2$, and get as an approximation:

$$\varepsilon(n_b) \simeq \varepsilon\left(\frac{n_+ + n_-}{2}\right). \tag{40}$$

The function $\Delta\varepsilon_s$ for the dielectrophoretic saturation condition can be calculated analytically from Eq. (40) by setting $n_s^- = 0$. Namely, at the surface, $\varepsilon_s(n_s^+, n_s^- = 0)$ and,

$$\begin{aligned}\Delta\varepsilon_s(n_s^+) &= \varepsilon_w - \frac{(\varepsilon_{\rm DPB}-\varepsilon_0)^2}{\varepsilon_{\rm DPB}^2}\frac{n_s^+ e^2}{2\pi k_B T c_d b}\\ &\times\left(4 - 5\frac{\kappa_D b}{2\pi}\tan^{-1}\frac{2\pi}{\kappa_D b} + \frac{1}{1+(\frac{2\pi}{\kappa_D b})^2}\right).\end{aligned} \tag{41}$$

From Eq. (11), the condition to satisfy for dielectrophoretic saturation is $\Delta\varepsilon_s(n_s^+) = 0$. However, this function in the DPB model is concave and approaches a positive definite value, $\Delta\varepsilon_s \to \varepsilon_{\rm DPB}$ as $n_s^+ \to \infty$. Hence, as can be observed from Fig. 11, the $\Delta\varepsilon_s(n_s^+)$ expression is always positive, and the dielectrophoretic saturation cannot occur for this permittivity function. In other words, for the Levy–Andelman–Orland permittivity model, the counter-ion saturation at high surface charge is always sterically-dominant.

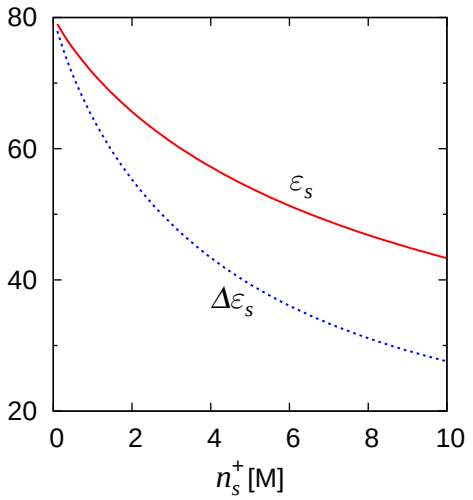

FIG. 11. The surface ε_s of the nonlinear permittivity model of Refs. 12 and 13, as in Eqs. (39) and (40) with $b = 0.264\,{\rm nm}$ (solid red line), and $\Delta\varepsilon_s$ (dashed blue line), Eq. (41), as a function of the counter-ion concentration at the surface, n_s^+. No dielectrophoretic saturation in the counter-ion concentration is seen as $\Delta\varepsilon_s > 0$ for the entire range of n_s^+.

Figure 12 shows a comparison between the linear decrement model as shown in Sec. III A, and the nonlinear decrement model of Eqs. (39) and (40). The counter-ion concentration in contact with a negatively charged surface, n_s^+, is plotted as a function of σ for KCl with $n_b = 10\,{\rm mM}$. For the linear decrement model, n_s^+ of the K^+ ions approaches the concentration of the dielectrophoretic saturation ($n_s^+ \simeq 4.89\,{\rm M}$) because for K^+, $d/a \simeq 1.05 > 1$, while for the nonlinear decrement model of Refs. 12 and 13, the surface counter-ion concentration approaches the closed-packing one of K^+, $n_s^+ \simeq 5.72\,{\rm M}$.

We conclude this section by comparing in Figure 13 the differential capacitance, C, as obtained in the linear decrement model, Eq. (8), and the nonlinear decrement one, of Eqs. (39) and (40). The calculations are done as a function of $\Psi_s < 0$ for KCl with $n_b = 10\,{\rm mM}$. For the nonlinear decrement model, the peak position occurs at higher Ψ_s than that for the linear decrement. This reflects the fact that the saturation of counter-ion concentration is dominated by steric effects. Moreover, due to the weaker permittivity decrement in the nonlinear model, the C value at the peak is higher than that for the linear decrement.

VI. CONCLUSIONS

We have presented the combined effect of ion finite-size and dielectric decrement on the electric double-layer (EDL) properties. The two important parameters are the surface charge density σ (or equivalently surface potential, ψ_s), and the salt concentration, n_b. Analytic expressions of the modified Grahame equation and the

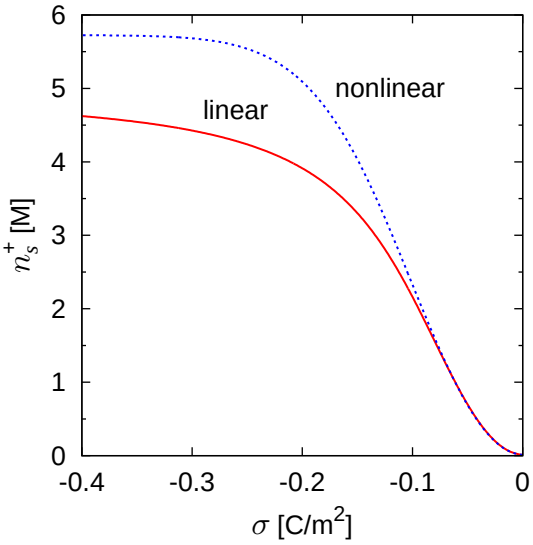

FIG. 12. Counter-ion concentration, n_s^+, in contact with a negatively charged surface, as a function of the surface charge density, σ, for KCl with $n_b = 10\,\mathrm{mM}$. The dotted (blue) line corresponds to the nonlinear permittivity decrement of Eqs. (39) and (40) with $b = 0.264$ nm, while the solid (red) line corresponds to the linear permittivity decrement, Eq. (8).

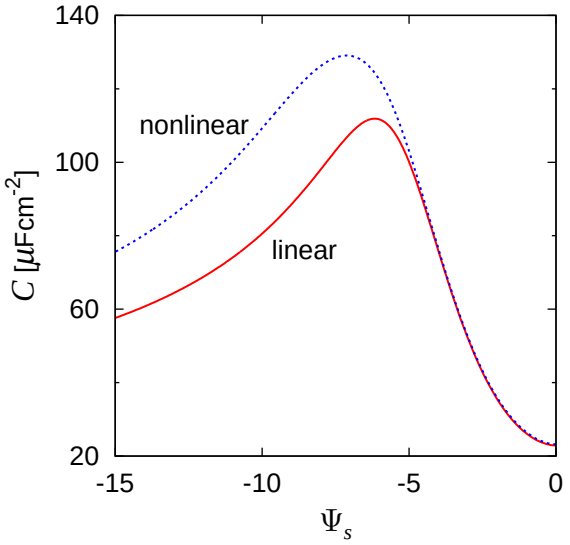

FIG. 13. Differential capacitance C for KCl with $n_b = 10\,\mathrm{mM}$, as function of negative Ψ_s. The blue dotted line denotes the nonlinear permittivity decrement of Eq. (39) with $b = 0.264\,\mathrm{nm}$, while the red solid line corresponds to a linear permittivity decrement.

differential capacitance C were derived, for several models of ionic-dependent permittivity, $\varepsilon(n_\pm)$.

We first treat the simpler linear decrement model, $\varepsilon(n_\pm) = \varepsilon_w - \gamma_+ n_+ - \gamma_- n_-$. The counter-ion concentration at the surface proximity, n_s, exhibits a saturation at high σ. It originates either from the steric or dielectric decrement effects. Within the linear decrement model, the dominant mechanism of the counter-ion saturation is ionic specific, and is determined by the relative size of $d = (2\gamma/\varepsilon_w)^{1/3}$ and the ionic finite size a. For $d > a$, the dielectric decrement dominates and the counter-ion concentration at the surface proximity saturates at the dielectrophoretic saturation, $n_s \simeq \varepsilon_w/2\gamma$, which then gives a lower and non-zero bound to the surface permittivity, $\varepsilon_s \simeq \varepsilon_w/2$. For $d < a$, although the dominant saturation is the steric one with $n_s \simeq 1/a^3$, the differential capacitance is found to be strongly affected by the dielectric decrement.

At low salt concentrations, whether the dominant mechanism for counter-ion saturation is dielectrophoretic or steric, the differential capacitance C exhibits a camel-shape as a function of ψ_s. This is obtained by our analytic and numerical results. In contrast, at high salt concentrations, the differential capacitance exhibits a skewed bell-shape, where the uni-modal peak is shifted from $\psi_s = 0$. This shift originates from the asymmetry between the cation and anion polarization properties.

We also discuss possible effects of nonlinear permittivity decrement on the dielectrophoretic saturation and differential capacitance. When a nonlinear $\varepsilon(n)$ is considered, the concentration at the dielectrophoretic saturation becomes larger than that of the linear decrement. Therefore, the effective length parameter d for the nonlinear model becomes smaller than for the linear decrement case. Moreover, the dielectrophoretic saturation does not exist when the permittivity decrement is too weak. In such a case, the peak in C always originates from the sterically-dominant saturation.

Finally, we would like to mention the possibility of direct experimental determination of the ionic specific dielectric decrement. In the past, measurements of the bulk permittivity have shown that $\varepsilon(n_b)$ depends on the salt concentration, n_b, but it was not possible to separate the contributions coming from the cations or anions. In order to evaluate the separate contribution of each ion type, appropriate physical quantity other than the bulk permittivity is required. The differential capacitance of the EDL at high surface potentials is one such candidate, because it essentially depends only on the dielectric decrement only by the counter-ions. The analytic relationship between the counter-ion specific decrement and the differential capacitance, Eqs. (35)-(37), would give a way to evaluation directly the ionic-specific dielectric decrement. Because our analytic results are valid for general nonlinear permittivity decrement, they can be used to determine nonlinear permittivity behavior for high ionic concentrations in contact with highly charged surfaces.

Acknowledgments We thank M. Bazant, M. Biesheuvel, C. Grosse, G. I. Guerrero-García and M. Olvera de la Cruz for useful discussions and numerous suggestions. The numerical calculations have been partly carried out using the computer facilities at the Research

Institute for Information Technology, Kyushu University. Y.N. would like to acknowledge support from the JSPS Institutional Program for Young Researcher Overseas Visits and the hospitality of Tel Aviv University where this project was initiated. This work has been supported by Grants-in-Aid for Scientific Research (JSPS KAKENHI) under Grant No. 26400433, the Israel Science Foundation (ISF) under Grant No. 438/12, and the U.S.-Israel Binational Science Foundation (BSF) under Grant No. 2012/060.

[1] *Soft Condensed Matter Physics in Molecular and Cell Biology*, edited by W. C. K. Poon and D. Andelman (Taylor & Francis, London, 2006).
[2] J. N. Israelachvili, *Intermolecular and Surface Forces*, 3rd ed. (Academic Press, Burlington, MA, 2011).
[3] H. A. Stone, A. D. Stroock, and A. Ajdari, Annu. Rev. Fluid Mech. **36**, 381 (2004).
[4] W. Sparreboom, A. van den Berg, and J. C. T. Eijkel, Nature Nano. **4**, 713 (2009).
[5] K. Jayalakshmi and M. Balasubramanian, Int. J. Electrochem. Sci. **3**, 1196 (2008).
[6] M. Z. Bazant, M. S. Kilic, B. D. Storey, and A. Ajdari, Adv. Colloid Interface Sci. **152**, 48 (2009).
[7] D. Henderson, L. Blum, and W. R. Smith, Chem. Phys. Lett. **63**, 381 (1979).
[8] P. Nielaba and F. Forstmann, Chem. Phys. Lett. **117**, 46 (1985).
[9] R. R. Netz and H. Orland, Euro. Phys. J. E **1**, 203 (2000).
[10] A. G. Moreira and R. R. Netz, EPL (Europhysics Letters) **52**, 705 (2000).
[11] A. Abrashkin, D. Andelman, and H. Orland, Phys. Rev. Lett. **99**, 077801 (2007).
[12] A. Levy, D. Andelman, and H. Orland, Phys. Rev. Lett. **108**, 227801 (2012).
[13] A. Levy, D. Andelman, and H. Orland, J. Chem. Phys. **139**, 164909 (2013).
[14] J. Clavilier and C. N. Van Huong, J. Electroanal. Chem. **80**, 101 (1977).
[15] G. Valette, J. Electroanal. Chem. **122**, 285 (1981).
[16] G. Valette, J. Electroanal. Chem. **138**, 37 (1982).
[17] J. J. Bikerman, Philos. Mag. **33**, 384 (1942).
[18] V. Kralj-Iglic and A. Iglic, Electrotechnical Rev. (Slovenia) **61**, 127 (1994).
[19] I. Borukhov, D. Andelman, and H. Orland, Phys. Rev. Lett. **79**, 435 (1997).
[20] A. A. Kornyshev, J. Phys. Chem. B **111**, 5545 (2007).
[21] M. S. Kilic, M. Z. Bazant, and A. Ajdari, Phys. Rev. E **75**, 021502 (2007).
[22] P. M. Biesheuvel and M. van Soestbergen, J. Colloid Interface Sci. **316**, 490 (2007).
[23] W. Dreyer, C. Guhlke, and R. Muller, Phys. Chem. Chem. Phys. **15**, 7075 (2013).
[24] W. Dreyer, C. Guhlke, and M. Landstorfer, Electrochem. Commun. **43**, 75 (2014).
[25] M. J. Sparnaay, *The Electrical Double Layer* (Pergamon, Oxford, 1972).
[26] P. M. Biesheuvel, Euro. Phys. J. E **16**, 353 (2005).
[27] D. Ben-Yaakov, D. Andelman, and R. Podgornik, J. Chem. Phys. **134**, 074705 (2011).
[28] M. M. Hatlo, R. van Roij, and L. Lue, Europhys. Lett. **97**, 28010 (2012).
[29] J. J. López-García, J. Horno, and C. Grosse, J. Colloid Interface Sci. **405**, 336 (2013).
[30] J. J. López-García, J. Horno, and C. Grosse, J. Colloid Interface Sci. **428**, 308 (2014).
[31] In Ref. 20, there is a misprint of factor 2. The condition should be: $2a^3 n_b > 1/4$.
[32] M. Islam, M. T. Alam, and T. Ohsaka, J. Phys. Chem. C **112**, 16568 (2008).
[33] G. I. Guerrero-García and M. Olvera de la Cruz, J. Chem. Theory Comput. **9**, 1 (2012).
[34] G. I. Guerrero-Garcia, Y. Jing, and M. Olvera de la Cruz, Soft Matter **9**, 6046 (2013).
[35] O. Stern, Z. Elektrochem. **30**, 508 (1924).
[36] D. C. Grahame, J. Am. Chem. Soc. **76**, 4819 (1954).
[37] D. J. Bonthuis and R. R. Netz, J. Phys. Chem. B **117**, 11397 (2013).
[38] J. B. Hasted, D. M. Ritson, and C. H. Collie, J. Chem. Phys. **16**, 1 (1948).
[39] The additivity assumption of separate ionic contributions as in Eq. (8) is not always fully obeyed. Experimental observations and molecular dynamic (MD) simulations of salt effects on ionic activity and air/water surface tension showed non-additive behavior of ions. This implies the existence of ion association caused by the difference in ion-solvent interactions between cations and anions. However, as precise modeling of $\varepsilon(n_\pm)$ is beyond the scope of this paper, we shall only focus on linear and nonlinear models for $\varepsilon(n_\pm)$, where the ionic contributions are taken to be additive. See, *e.g.,* L. Yang, Y. Fan, and Y. Q. Gao, J. Phys. Chem. B **115**, 12456 (2011); Y. Q. Gao, J. Phys. Chem. B **115**, 12466 (2011); W. J. Xie and Y. Q. Gao, J. Phys. Chem. Lett. **4**, 4247 (2013).
[40] E. R. Nightingale, J. Phys. Chem. **63**, 1381 (1959).
[41] M. Kilic, M. Bazant, and A. Ajdari, Phys. Rev. E **75**, 021503 (2007).
[42] Y. Z. Wei and S. Sridhar, J. Chem. Phys. **92**, 923 (1990).
[43] Y.-Z. Wei, P. Chiang, and S. Sridhar, J. Chem. Phys. **96**, 4569 (1992).